Analysis of three-body hadronic *D*-meson decays

Xu-Da Zhou and Si-Hong Zhou*

Inner Mongolia Key Laboratory of Microscale Physics and Atom Innovation, School of Physical Science and Technology, Inner Mongolia University, Hohhot 010021, China and Center for Quantum Physics and Technologies, School of Physical Science and Technology, Inner Mongolia University, Hohhot 010021, China

(Received 27 March 2025; accepted 30 May 2025; published 11 June 2025)

Motivated by recent experimental advances in three-body hadronic D decays from BESIII, we present a systematic analysis of $D_{(s)} \to P_1(V \to)P_2P_3$ decay processes, where V denotes vector resonances (ρ, K^*, ω, ϕ) and $P_{1,2,3}$ are light pseudoscalar mesons ($\pi, K, \eta^{(\prime)}$). Using the factorization-assisted topological-amplitude (FAT) approach, we calculate the intermediate subprocesses $D_{(s)} \to P_1V$, incorporating relativistic Breit-Wigner distributions to model the subsequent $V \to P_2P_3$ strong decays. By comprehensively including all relevant resonances (ρ, K^*, ω, ϕ), we calculate branching fractions for these decay modes as well as the Breit-Wigner-tail effects in $D_{(s)} \to P_1(\omega \to)KK$ processes. Our framework comprehensively incorporates both factorizable and nonfactorizable contributions, significantly improving theoretical predictions in the nonperturbative regime where conventional methods face challenges due to the limited mass scale of charm mesons. The FAT approach yields results in good agreement with experimental data, demonstrating its effectiveness in capturing nonfactorizable contributions with improved precision. Our predictions for yet-unobserved decay modes, particularly those with branching fractions in the order of 10^{-4}–10^{-3}, are expected to be tested in future high-precision experiments at BESIII and LHCb.

DOI: 10.1103/rqbl-zdhj

I. INTRODUCTION

Hadronic charm decays are important for probing the dynamics of both strong and weak interactions in the low-energy regime. Particularly in multibody D-meson decays, such as three-body modes, with nontrivial kinematics and phase space distributions, they offer valuable opportunities for exploring hadron spectroscopy as the invariant mass squared of two final-state particles often peaks, revealing resonances at the edges of the Dalitz plot.

Experimentally, measurements of the branching fractions and CP asymmetries of hadronic D-meson decays, by BESIII [1–6], LHCb [7–11], CLEO [12–19], Belle (II) [20,21], and *BABAR* [22–26], offer direct insights into the amplitudes and phases involved in the decay process. For multibody D-meson decays, in addition to the absolute branching fractions obtained in Refs. [1–6,13,23], the fit fractions of each resonance and nonresonance components can also be measured. This can be done using the amplitude analysis with the Dalitz plot technique where the resonances are parametrized as the relativistic Breit-Wigner (RBW) model and nonresonant terms by exponential distributions. Especially, three-body D-meson decays were predicted to occur primarily through intermediate quasi-two-body states in Ref. [27], which aligns with the experimentally observed pattern [22,25,28]. The experimental measurements of these quasi-two-body decays provide new information on the resonances.

On the theoretical side, given that the charm quark mass m_c is not heavy enough and $1/m_c$ power corrections are so large that a reliable heavy quark expansion becomes impractical, the QCD-inspired approaches, such as QCD factorization (QCDF) [29] and perturbative QCD (PQCD) [30,31] applied successfully in hadronic B decays might not be suitable for describing hadronic decays of the D meson. The studies of D-meson decays involve application of approximate flavor symmetries, such as flavor $SU(3)_F$ [32–34] for three-body decays, topological diagrams for two-body modes [35–42], and its implication in three-body decays [43], the factorization-assisted topological-amplitude (FAT) approach for two- [44–46] and three-body decays [47,48], SU(2)-subgroup symmetry, U spin [49], and a series of works on scalar resonance in three-body D-meson decays using flavor $SU(3)_F$ [50–57]. A phenomenological approach based on QCDF for

*Contact author: shzhou@imu.edu.cn

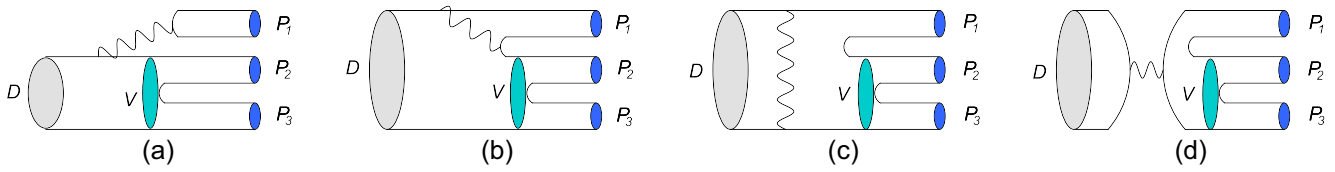

FIG. 1. Typical topological diagrams of $D_{(s)} \to P_1(V \to)P_2P_3$ under the framework of quasi-two-body decay with the wavy line representing a W boson: (a) color-favored tree diagram T, (b) color-suppressed tree diagram C, (c) W-exchange tree diagram E, and (d) W-annihilation tree diagram A.

three-body hadronic D-meson decay amplitudes can be found in Refs. [58–61], while the approaches using more complex theoretical background in Faddeev techniques and Khuri-Treiman and triangle singularities are discussed in [62–65], and an inverse problem approach is discussed in [66,67]. As mentioned at the beginning, since the low-energy scale involved in D-meson decay processes, the theoretical studies on D-meson decays remain relatively limited.

In this work, we focus on three-body D-meson decays $D_{(s)} \to P_1(V \to)P_2P_3$, where V represents a vector resonant, ρ, K^*, ω, ϕ, and $P_{1,2,3}$ are light pseudoscalar mesons, specifically pion, kaon, and $\eta^{(\prime)}$. These decays are often referred to quasi-two-body decays, as two of the three final-state particles P_2 and P_3 originate from an intermediate vector resonance V, while the third meson P_1, referred to as the "bachelor" meson, recoils against the resonance system. Such processes typically manifest at the edges of the Dalitz plot, and their amplitude analyses are accessible in experiments. BESIII Collaborations have performed the amplitude analysis and measured the partial branching fractions of quasi-two-body D decays, such as $D^+ \to K^0_S\pi^+\pi^-$, $D^+ \to K^0_S\pi^+\pi^0$, and $D^+_s \to K^+\pi^+\pi^-$ with ρ and $\bar{K}^*$ as intermediate resonances [68,69], $D^0 \to K^0_S(\phi \to)K^+K^-$ [70], $D^+_s \to \pi^+(K^*, \phi \to)K^+K^-$ [71], $D^+_s \to K^0_S(\rho, K^* \to)\pi^+\pi^0$ [72], $D^+ \to K^0_S(K^* \to)K^+\pi^0$ [73], and doubly Cabibbo-suppressed decays $D^+ \to \pi^0/\eta(K^* \to)K^+\pi^0$ [74], $D^+_s \to \eta'(\rho \to)\pi^+\pi^0$ [75]. LHCb Collaborations have investigated structures of vector resonance $\bar{K}^{*0}, \phi$ with their corresponding fit fractions through $D^+ \to K^-K^+\pi^+$ [7]. This experimental information on $D_{(s)} \to P_1(V \to)P_2P_3$ can be used to explore the resonant substructure and understand strong dynamics of final particles.

For the systematic study of $D_{(s)} \to P_1(V \to)P_2P_3$ decays, we will apply the FAT approach. It was initially proposed just to address the issue of nonfactorizable contributions in two-body D and B meson decays by one of us (S.-H. Zhou and coworkers [44–46,76–81]), and we have subsequently extended it to describe quasi-two-body B meson decays [81–83]. This theoretical framework is built upon the conventional topological diagram approach [36], which categorizes decay amplitudes according to distinct electroweak Feynman diagrams while retaining SU(3) breaking effects. It incorporates SU(3) asymmetries into topological diagram amplitudes primarily through form factors and decay constants, assisted by QCD factorization. The remaining contributions are treated as a small number of unknown nonfactorization parameters, which are determined through a global fit to all available experimental data. Thanks to recent measurements of various $D \to PV$ decay modes with a significantly improved precision measured by BESIII, particularly with the addition of some single and doubly Cabibbo-suppressed modes, we have updated the analysis of $D \to PV$ decays in the FAT approach [84]. By incorporating these new and precise data of Cabibbo-favored, single Cabibbo-suppressed, and doubly Cabibbo-suppressed modes, we have refitted the nonfactorizable parameters. This global fit analysis differs from the previous results obtained using the topological diagram approach, which was limited to Cabibbo-favored mode data and led to many solutions of the topological amplitude parameters with similarly small local minima in χ^2 in Ref. [85]. Consequently, the FAT approach now provides the most accurate decay amplitudes for two-body D meson decays. We will use the updated nonfactorizable parameters to calculate the branching fractions of quasi-two-body D decays, while leave the issue of CP asymmetries arising from interference between tree and penguin processes for the future work, owing to the lack of knowledge on precise results of penguin contributions.

The remainder of this paper is organized as follows. In Sec. II, the theoretical framework is introduced. Numerical results and detailed discussions are given in Sec. III. Section IV has our conclusions.

II. FACTORIZATION AMPLITUDES FOR TOPOLOGICAL DIAGRAMS

The quasi-two-body process, $D_{(s)} \to P_1P_2P_3$ decay is divided into two sequential stages. First, the $D_{(s)}$ meson decays into P_1 and an intermediate vector resonance V. Subsequently, the vector resonance V decays into the final-state particles P_2P_3. The first decay, $D_{(s)} \to P_1V$, is a weak decay induced by quark-level transition $c \to d(s)u\bar{d}(\bar{s})$ at leading order in the electroweak interaction, and by $c \to uq\bar{q}(q = u, d, s)$ in penguin diagrams. However, since the penguin amplitudes are suppressed by Wilson coefficients and Cabibbo-Kobayashi-Maskawa (CKM) matrix

elements, they can be neglected in the calculation of branching fractions. The secondary decay $V \to P_2P_3$ proceeds via strong interaction with the vector resonance described by the RBW model. The two-step decays of the D meson, $D_{(s)} \to P_1P_2P_3$, can be described by topological diagrams under the framework of quasi-two-body decay at tree level, as shown in Fig. 1. These diagrams include (a) color-favored emission diagram T, (b) color-suppressed emission diagram C, (c) W-exchange diagram E, and (d) W-annihilation diagram A, which are characterized by topological structures of the weak interaction. In these figures, we only illustrate the case that the intermediate resonance (labeled by green ovals) is produced as a recoiling particle in emission diagrams, while the scenario of the intermediate resonance being emitted is not shown.

First, we review the intermediate two-body decay amplitudes of these four diagrams within the FAT approach. Compared to B-meson decays, more large nonfactorizable contributions are exhibited in D mesons due to the lower energy scale involved. Even for the T diagram, it is necessary to introduce an additional unknown parameter to account for its nonfactorizable effects, as would have been discussed in Ref. [84]. A detailed explanation of the parametrization of the amplitudes for the T, C, E, and A topologies can be found in Ref. [45] and these amplitudes are expressed as follows:

$$\begin{aligned}
T_{P_1V}(C_{P_1V}) &= \sqrt{2}G_F V_{cq}^* V_{uq'} a_1(\mu)(a_2^V(\mu)) f_V m_V \\
&\quad \times F_1^{DP_1}(m_V^2)(\varepsilon_V^* \cdot p_D), \\
T_{VP_1}(C_{VP_1}) &= \sqrt{2}G_F V_{cq}^* V_{uq'} a_1(\mu)(a_2^P(\mu)) f_{P_1} m_V \\
&\quad \times A_0^{DV}(m_{P_1}^2)(\varepsilon_V^* \cdot p_D), \\
E_{P_1V,VP_1} &= \sqrt{2}G_F V_{cq}^* V_{uq'} C_2(\mu) \chi_{q(s)}^E e^{i\phi_{q(s)}^E} f_D \\
&\quad \times m_V \frac{f_{P_1} f_V}{f_\pi f_\rho}(\varepsilon_V^* \cdot p_D), \\
A_{P_1V,VP_1} &= \sqrt{2}G_F V_{cq}^* V_{uq'} C_1(\mu) \chi_{q(s)}^A e^{i\phi_{q(s)}^A} f_D \\
&\quad \times m_V \frac{f_{P_1} f_V}{f_\pi f_\rho}(\varepsilon_V^* \cdot p_D),
\end{aligned} \tag{1}$$

with

$$\begin{aligned}
a_1(\mu) &= C_2(\mu) + C_1(\mu)\left(\frac{1}{N_C} + \chi^T\right), \\
a_2^{V(P)}(\mu) &= C_1(\mu) + C_2(\mu)\left(\frac{1}{N_C} + \chi_{V(P)}^C e^{i\phi_{V(P)}^C}\right),
\end{aligned} \tag{2}$$

where $N_C = 3$. The scale μ of the Wilson coefficients is set to the energy release in individual decay modes as indicated by the PQCD approach [30,31]: it is dependent on the mass scales of initial and final states and strong binding energy parameter $\Lambda_{\rm QCD}$. It is defined as

$$\mu = \sqrt{\Lambda_{\rm QCD} m_D (1 - r_{P(V)}^2)}, \tag{3}$$

for emission diagrams (T and C), and

$$\mu = \sqrt{\Lambda_{\rm QCD} m_D (1 - r_P^2)(1 - r_V^2)}. \tag{4}$$

for annihilation diagrams (E and A), respectively, where $r_{P(V)} = m_{P(V)}/m_D$ is the mass ratio of the emitted pseudoscalar (vector) meson from the weak vertex to the D meson.

In Eq. (1), the subscripts P_1V, VP_1 are used to distinguish between cases where the recoiling meson (the first particle) is a pseudoscalar or a vector meson. The quark in the CKM matrix element is denoted as $q^{(\prime)} = d$, s. The polarization vector of vector meson V is represented by ε_V^*. The decay constants of the mesons P_1 and V are given by f_{P_1} and f_V, respectively. The vector form factors for transitions $D_{(s)} \to P_1$ and $D_{(s)} \to V$ are denoted by $F_1^{DP_1}$ and A_0^{DV}, respectively. The parameters $\chi^T, \chi_{V(P)}^C, \chi_{q(s)}^E$, and $\chi_{q(s)}^A$ are related to the magnitudes of topological diagrams T, C, E, and A, respectively, associated with their corresponding strong phases $\phi_{V(P)}^C, \phi_{q(s)}^E$, and $\phi_{q(s)}^A$, needed to be fitted globally from the experimental data. In order to minimize the number of free parameters, we do not introduce a strong phase for the T diagram, as we only consider its phase relative to other diagrams. For the C diagram, we introduce two distinct sets of parameters: χ_V^C, ϕ_V^C and χ_P^C, ϕ_P^C, to account for whether the emitted meson is a vector (V) or a pseudoscalar (P) particle. Additionally, the subscripts q and s in $\chi_{q(s)}^E, \chi_{q(s)}^A, \phi_{q(s)}^E$, and $\phi_{q(s)}^A$ are used to differentiate between the strongly produced light-quark pair (u or d) and the strange-quark pair. This distinction, which indicates the $SU(3)$ breaking effect, is crucial for accurately describing the dynamics of the decay processes of E and A diagrams. For the two annihilation amplitudes, it is also noted that the Glauber phase S_π is introduced as an additional strong phase arising from their nonfactorizable contributions, when a pion is involved in the final state [44,45]. This strong phase plays a more crucial role in the interference between the emission diagrams and the annihilation ones, particularly with the availability of more precise experimental data [84].

The secondary subprocess $V \to P_2P_3$ is described using the RBW line shape, which is widely applied in both experimental data analyses and theoretical modeling of resonances, ρ, K^*, ω, and ϕ in the strong decay process [69,72,75,86–91]. The explicit expression of RBW distribution is written as

$$L^{\rm RBW}(s) = \frac{1}{s - m_V^2 + i m_V \Gamma_V(s)}, \tag{5}$$

where $s = m_{23}^2 = (p_2 + p_3)^2$ is the invariant mass squared of the two-body system, with p_2 and p_3 denoting the

4-momenta of the two mesons P_2 and P_3 moving collinearly, respectively. The energy-dependent width of the vector resonance $\Gamma_V(s)$ is defined as

$$\Gamma_V(s) = \Gamma_0 \left(\frac{q}{q_0}\right)^3 \left(\frac{m_V}{\sqrt{s}}\right) X^2(qr_{\rm BW}), \tag{6}$$

where q is the momentum magnitude of either P_2 or P_3 in the rest frame of the resonance V, given by

$$q = \frac{1}{2}\sqrt{[s-(m_{P_2}+m_{P_3})^2][s-(m_{P_2}-m_{P_3})^2]/s}, \tag{7}$$

and q_0 is the value of q when $s = m_V^2$. The Blatt-Weisskopf barrier factor $X(qr_{\rm BW})$ is defined as [92]

$$X(qr_{\rm BW}) = \sqrt{[1+(q_0 r_{\rm BW})^2]/[1+(qr_{\rm BW})^2]}. \tag{8}$$

In cases where the pole mass m_V lies outside the kinematics region, i.e., $m_V < m_{P_2} + m_{P_3}$, the mass m_V is replaced with an effective mass $m_V^{\rm eff}$, calculated using the *ad hoc* formula [93,94]

$$m_V^{\rm eff}(m_V) = m^{\rm min} + (m^{\rm max} - m^{\rm min}) \times \left[1 + \tanh\left(\frac{m_V - \frac{m^{\rm min}+m^{\rm max}}{2}}{m^{\rm max}-m^{\rm min}}\right)\right], \tag{9}$$

where $m^{\rm max}$ and $m^{\rm min}$ are the upper and lower boundaries of the kinematic region, respectively. The barrier radius $r_{\rm BW} = 4.0({\rm GeV})^{-1}$ is used for all resonances [95]. The masses m_V and full widths Γ_0 of the resonances are taken from Particle Data Group (PDG) [96] and are listed in Table I.

Finally the intermediate resonance V described above decays via strong interaction, with the matrix element $\langle P_2(p_2)P_3(p_3)|V(p_V)\rangle$ parametrized as a strong coupling constant $g_{VP_2P_3}$. This coupling constant can be extracted from the measured partial decay widths $\Gamma_{V\to P_2P_3}$ using the relations

TABLE I. Masses m_V and full widths Γ_0 of vector resonant states.

Resonance	Line shape parameters (MeV)	Resonance	Line shape parameters (MeV)
$\rho(770)$	$m_V = 775.26$ $\Gamma_0 = 149.1$	$\omega(782)$	$m_V = 782.65$ $\Gamma_0 = 8.49$
$K^*(892)^+$	$m_V = 891.66$ $\Gamma_0 = 50.8$	$K^*(892)^0$	$m_V = 895.55$ $\Gamma_0 = 47.3$
$\phi(1020)$	$m_V = 1019.46$ $\Gamma_0 = 4.25$		

$$\Gamma_{V\to P_2P_3} = \frac{2}{3}\frac{p_c^3}{4\pi m_V^2} g^2_{V\to P_2P_3}, \tag{10}$$

where p_c is the magnitude of pseudoscalar meson momentum in the rest frame of the vector meson. The numerical values of the strong coupling constants $g_{\rho\to\pi^+\pi^-}$, $g_{K^*\to K^+\pi^-}$ and $g_{\phi\to K^+K^-}$ have already been determined from experimental data [97],

$$g_{\rho\to\pi^+\pi^-} = 6.0, \quad g_{K^*\to K^+\pi^-} = 4.59, \quad g_{\phi\to K^+K^-} = -4.54. \tag{11}$$

Other strong coupling constants can be derived from these results using relationships based on the quark model result [98]. These relationships are

$$g_{\rho\to K^+K^-} : g_{\omega\to K^+K^-} : g_{\phi\to K^+K^-} = 1:1:-\sqrt{2},$$
$$g_{\rho^0\pi^+\pi^-} = g_{\rho^+\pi^0\pi^+}, \quad g_{\rho^0\pi^0\pi^0} = g_{\omega\pi^+\pi^-} = 0,$$
$$g_{\rho^0K^+K^-} = -g_{\rho^0K^0\bar{K}^0} = g_{\omega K^+K^-} = g_{\omega K^0\bar{K}^0}, \quad g_{\phi K^+K^-} = g_{\phi K^0\bar{K}^0}.$$

Combining the two subprocesses together for $D_{(s)} \to P_1(V\to)P_2P_3$, the decay amplitudes of the four topological diagrams shown in Fig. 1 are listed in the following:

$$\begin{aligned}
T_{(P_2P_3)P_1} &= \langle P_2(p_2)P_3(p_3)|(\bar{q}c)_{V-A}|D(p_D)\rangle\langle P_1(p_1)|(\bar{u}q')_{V-A}|0\rangle \\
&= \frac{\langle P_2(p_2)P_3(p_3)|V(p_V)\rangle}{s-m_V^2+im_V\Gamma_V(s)}\langle V(p_V)|(\bar{q}c)_{V-A}|D(p_D)\rangle\langle P_1(p_1)|(\bar{u}q')_{V-A}|0\rangle \\
&= 2\mathbf{p_1}\cdot\mathbf{p_2}\sqrt{2}G_F V_{cq}^* V_{uq'} a_1(\mu) f_{P_1} m_V A_0^{DV}(m_{P_1}^2)\frac{g_{VP_2P_3}}{s-m_V^2+im_V\Gamma_V(s)}, \\
T_{P_1(P_2P_3)} &= \langle P_2(p_2)P_3(p_3)|(\bar{u}q')_{V-A}|0\rangle\langle P_1(p_1)|(\bar{q}c)_{V-A}|D(p_D)\rangle \\
&= \frac{\langle P_2(p_2)P_3(p_3)|V(p_V)\rangle}{s-m_V^2+im_V\Gamma_V(s)}\langle V(p_V)|(\bar{q}c)_{V-A}|0\rangle\langle P_1(p_1)|(\bar{u}q')_{V-A}|D(p_D)\rangle \\
&= 2\mathbf{p_1}\cdot\mathbf{p_2}\sqrt{2}G_F V_{cq}^* V_{uq'} a_1(\mu) f_V m_V F_1^{DP_1}(s)\frac{g_{VP_2P_3}}{s-m_V^2+im_V\Gamma_V(s)},
\end{aligned} \tag{12}$$

$$
\begin{aligned}
C_{(P_2P_3)P_1} &= \langle P_2(p_2)P_3(p_3)|(\bar{q}'c)_{V-A}|D(p_D)\rangle\langle P_1(p_1)|(\bar{u}q)_{V-A}|0\rangle \\
&= \frac{\langle P_2(p_2)P_3(p_3)|V(p_V)\rangle}{s-m_V^2+im_V\Gamma_V(s)}\langle V(p_V)|(\bar{q}'c)_{V-A}|D(p_D)\rangle\langle P_1(p_1)|(\bar{u}q)_{V-A}|0\rangle \\
&= 2\mathbf{p_1}\cdot\mathbf{p_2}\sqrt{2}G_F V_{cq}^* V_{uq'} a_2^P(\mu) f_{P_1} m_V A_0^{DV}(m_{P_1}^2)\frac{g_{VP_2P_3}}{s-m_V^2+im_V\Gamma_V(s)}, \\
C_{P_1(P_2P_3)} &= \langle P_2(p_2)P_3(p_3)|(\bar{u}q)_{V-A}|0\rangle\langle P_1(p_1)|(\bar{q}'c)_{V-A}|D(p_D)\rangle \\
&= \frac{\langle P_2(p_2)P_3(p_3)|V(p_V)\rangle}{s-m_V^2+im_V\Gamma_V(s)}\langle V(p_V)|(\bar{u}q)_{V-A}|0\rangle\langle P_1(p_1)|(\bar{q}'c)_{V-A}|D(p_D)\rangle \\
&= 2\mathbf{p_1}\cdot\mathbf{p_2}\sqrt{2}G_F V_{cq}^* V_{uq'} a_2^V(\mu) f_V m_V F_1^{DP_1}(s)\frac{g_{VP_2P_3}}{s-m_V^2+im_V\Gamma_V(s)},
\end{aligned}
\tag{13}
$$

$$
\begin{aligned}
E_{P_1(P_2P_3)} &= \langle P_1(p_1)P_2(p_2)P_3(p_3)|\mathcal{H}_{\rm eff}|D(p_D)\rangle \\
&= \frac{\langle P_2(p_2)P_3(p_3)|V(p_V)\rangle}{s-m_V^2+im_V\Gamma_V(s)}\langle V(p_V)P_1(p_1)|\mathcal{H}_{\rm eff}|D(p_D)\rangle \\
&= 2\mathbf{p_1}\cdot\mathbf{p_2}\sqrt{2}G_F V_{cq}^* V_{uq'} C_2(\mu)\chi_{q(s)}^E e^{i\phi_{q(s)}^E} f_D m_V \frac{f_V f_{P_1}}{f_\pi f_\rho}\frac{g_{VP_2P_3}}{s-m_V^2+im_V\Gamma_V(s)}, \\
A_{P_1(P_2P_3)} &= \langle P_1(p_1)P_2(p_2)P_3(p_3)|\mathcal{H}_{\rm eff}|D(p_D)\rangle \\
&= \frac{\langle P_2(p_2)P_3(p_3)|V(p_V)\rangle}{s-m_V^2+im_V\Gamma_V(s)}\langle V(p_V)P_1(p_1)|\mathcal{H}_{\rm eff}|D(p_D)\rangle \\
&= 2\mathbf{p_1}\cdot\mathbf{p_2}\sqrt{2}G_F V_{cq}^* V_{uq'} C_1(\mu)\chi_{q(s)}^A e^{i\phi_{q(s)}^A} f_D m_V \frac{f_V f_{P_1}}{f_\pi f_\rho}\frac{g_{VP_2P_3}}{s-m_V^2+im_V\Gamma_V(s)},
\end{aligned}
\tag{14}
$$

where the prefactor $2\mathbf{p_1}\cdot\mathbf{p_2}$ in these amplitudes is derived in the rest frame of the P_2P_3 system. In the decay process $D_{(s)}\to P_1(V\to)P_2P_3$, where $p_V=p_2+p_3=\sqrt{s}$, the form factor $F_1^{DP_1}(s)$ depends on the invariant mass s of the P_2P_3 system. This is in contrast to two-body decays, where the form factor is evaluated at a fixed value of s (typically $s=m_V^2$, the mass of the vector meson).

The matrix element for the decay $D_{(s)}\to P_1P_2P_3$ can be expressed in the form

$$
\langle P_1(p_1)P_2(p_2)P_3(p_3)|\mathcal{H}_{\rm eff}|D_{(s)}(p_D)\rangle = 2\mathbf{p_1}\cdot\mathbf{p_2}\mathcal{A}(s), \tag{15}
$$

where $\mathcal{A}(s)$ represents the summation of amplitudes in Eqs. (12)–(14) with the prefactor $2\mathbf{p_1}\cdot\mathbf{p_2}$ factored out. The differential decay width for $D_{(s)}\to P_1P_2P_3$ is given by

$$
d\Gamma = ds\frac{1}{(2\pi)^3}\frac{(|\mathbf{p_1}||\mathbf{p_2}|)^3}{6m_D^3}|\mathcal{A}(s)|^2, \tag{16}
$$

where the magnitudes $|\mathbf{p_1}|$ and $|\mathbf{p_2}|$ of the three-momenta of the particles P_1 and P_2 are evaluated in the rest frame of the P_2P_3 system. The expression for $|\mathbf{p_1}|$ is

$$
|\mathbf{p_1}| = \frac{1}{2\sqrt{s}}\sqrt{[(m_D^2-m_{P_1}^2)^2]-2(m_D^2+m_{P_1}^2)s+s^2}, \tag{17}
$$

and $|\mathbf{p_2}|=q$, corresponding to the momentum of P_2 (or P_3), in the P_2P_3 system rest frame, as defined in Eq. (6).

III. NUMERICAL RESULTS OF BRANCHING FRACTIONS

The input parameters are categorized as follows:

(1) Electroweak coefficients: These include the CKM matrix elements and Wilson coefficients.
   (a) The CKM matrix elements are provided in the PDG [96].
   (b) The Wilson coefficients $C_{1(2)}(\mu)$ [see Eq. (2)] for D-meson decays are taken from Eqs. (B1), (B2), and (B7) in the Appendix of Ref. [44]. The scale μ in $C_{1(2)}(\mu)$ is dependent on masses involved in each decay mode and the soft scale in the D meson, $\Lambda_{\rm QCD}$, as in Eqs. (3) and (4).

(2) Hadronic parameters: The parameters m_V, Γ_0 involved in the strong interaction decays of vector mesons have been listed in Table I. The strong coupling constants $g_{VP_2P_3}$ are presented in Eq. (11), along with the associated relationships provided below.

TABLE II. Decay constants of pseudoscalar and vector mesons.

f_π	f_K	f_D	f_{D_s}	f_ρ	f_{K^*}	f_ω	f_ϕ
130.2 ± 1.7	155.6 ± 0.4	211.9 ± 1.1	258 ± 12.5	213 ± 11	220 ± 11	192 ± 10	225 ± 11

(3) Nonperturbative QCD parameters: These encompass decay constants, transition form factors, and nonfactorizable parameters $\chi^T, \chi^C_{V(P)}, \chi^E_{q(s)}, \chi^A_{q(s)}$ and $\phi^C_{V(P)}, \phi^E_{q(s)}, \phi^A_{q(s)}, S_\pi$.

(a) The decay constants of light pseudoscalar mesons and vector mesons (in units of MeV) are listed in Table II. The decay constants of π, K, and $D_{(s)}$ are obtained from the PDG [96]. For the decay constants of vector mesons that have not been experimentally measured, we adopt the same theoretical values as used in quasi-two-body decays of B mesons [82,83], keeping a 5% error.

(b) The transition form factors of D-meson decays, specifically $D \to \pi$ and $D \to K$, have been measured by several experiments, including CLEO-c [99], Belle [100], and BESIII [101,102]. While most form factors have not been measured in experiments, theoretical predictions are available from various theoretical methods, such as lattice QCD [103], QCD sum rule [104,105], quark model [106], covariant light-front quark model [107–109], improved light-cone harmonic oscillator model [110], heavy meson and chiral symmetries (HM$_\chi$T) [111], hard-wall AdS/QCD model [112], and four-flavor holographic QCD [113]. Since different theoretical approaches yield varying values of the form factors, we adopt their values at zero recoil momentum ($Q^2 = 0$) within the range of experimental and theoretical results and assign a 10% error bar to account for uncertainties. As will be demonstrated in the following section, the form factor uncertainty constitutes the major source of theoretical uncertainty in our calculation. These values, along with α_i parameters, are presented in Table III. The Q^2 dependence of these form factors is uniformly parametrized using a dipole form, as follows:

$$F_i(Q^2) = \frac{F_i(0)}{1 - \alpha_1 \frac{Q^2}{m^2_{\rm pole}} + \alpha_2 \frac{Q^4}{m^4_{\rm pole}}}, \tag{18}$$

where F_i represents form factor F_1 or A_0, and $m_{\rm pole}$ is the mass of the corresponding pole state, e.g., m_{D^*} for $F_1^{D\pi, D\eta^{(\prime)}, D_s K}$, $m_{D_s^*}$ for $F_1^{DK, D_s\eta^{(\prime)}}$, m_D for $A_0^{D\rho, D\omega, D_s K^*}$, and m_{D_s} for $A_0^{DK^*, D_s\phi}$. The dipole model parameters $\alpha_{1,2}$ can be found in Table II of [114].

(c) The nonfactorizable parameters of the topological diagram amplitudes in Eqs. (12)–(14) consist of 15 free parameters: $\chi^T, \chi^C_{V(P)}, \chi^E_{q(s)}$, and $\chi^A_{q(s)}$, along with their associated phases $\phi^C_{V(P)}$, $\phi^E_{q(s)}, \phi^A_{q(s)}$, S_π [the factor e^{iS_π} multiplies the $E(A)_{P_1(P_2P_3)}$ terms in Eq. (14)] and the soft scale $\Lambda_{\rm QCD}$ [see Eqs. (3) and (4)]. These parameters are extracted through a global fit to 41 experimental data of $D \to PV$ with significance exceeding 3σ, as updated in Ref. [84]. The best-fitted parameters together with their corresponding uncertainties are

$$\begin{aligned}
&\chi^T = -0.29 \pm 0.01, \\
&\chi^C_P = -0.47 \pm 0.02, \quad \phi^C_P = 0.37 \pm 0.12, \\
&\chi^C_V = -0.41 \pm 0.01, \quad \phi^C_V = -0.52 \pm 0.02, \\
&\chi^E_q = 0.13 \pm 0.01, \quad \phi^E_q = 2.68 \pm 0.10, \\
&\chi^E_s = 0.24 \pm 0.01, \quad \phi^E_s = 3.52 \pm 0.07, \\
&\chi^A_q = 0.10 \pm 0.003, \quad \phi^A_q = -2.08 \pm 0.16, \\
&\chi^A_s = 0.18 \pm 0.01, \quad \phi^A_s = 2.62 \pm 0.10, \\
&\Lambda_{\rm QCD} = (0.24 \pm 0.01)\,{\rm GeV}, \quad S_\pi = -1.80 \pm 0.17,
\end{aligned} \tag{19}$$

with the fitted $\chi^2 = 6.2$ degrees of freedom. These nonfactorizable parameters are highly precise, with the exception of the strong phase ϕ^C_P. As is known, ϕ^C_P is primarily constrained by data from modes dominated by the C_{VP} diagram. Specifically, those involving only the C_{VP} term or

TABLE III. Form factors and dipole model parameters.

	$F_1^{D\to\pi}$	$F_1^{D\to K}$	$F_1^{D_s\to K}$	$F_1^{D\to\eta_q}$	$F_1^{D\to\eta_s}$
$F_i(0)$	0.60	0.74	0.66	0.76	0.79
α_1	1.24	1.33	1.20	1.03	1.23
α_2	0.24	0.33	0.20	0.29	0.23
	$A_0^{D\to\rho}$	$A_0^{D\to K^*}$	$A_0^{D_s\to K^*}$	$A_0^{D\to\omega}$	$A_0^{D_s\to\phi}$
$F_i(0)$	0.84	0.73	0.68	0.68	0.70
α_1	1.36	1.17	1.20	1.36	1.10
α_2	0.36	0.17	0.20	0.36	0.10

accompanied by minor contributions from annihilation diagrams. However, the experimental data for such modes remain scarce, limiting the precision of ϕ_P^C. Using the fitted parameters $\chi^T, \chi^C_{V(P)}, \phi^C_{V(P)}$, we calculate the values of $a_1(\mu)$ and $a_2^{V(P)}(\mu)$ for the emission diagrams of each decay modes. For instance, in the decay $D^+ \to \bar{K}^0(\rho^+)\pi^+\pi^-$, we determine $a_1(\mu), a_2^V(\mu)$, alongside the corresponding Wilson coefficients of $C_{1(2)}(\mu)$ at fixed scale μ relevant to this process,

$$\begin{aligned} &\mu = 0.61 \text{ GeV}, \\ &C_1(\mu) = -0.81, \qquad C_2(\mu) = 1.49, \\ &a_1(\mu) = -1.45, \qquad a_2^V(\mu) = 1.09e^{i0.26}. \end{aligned} \tag{20}$$

The branching fractions of $D_{(s)} \to P_1(V \to)P_2P_3$ can be obtained by integrating the differential width given in Eq. (16) over the region of s. Our numerical results for the branching fractions of $D_{(s)}$ decays are collected in Tables IV–VII, corresponding to the processes $D_{(s)} \to P_1\rho \to P_1\pi\pi$, $D_{(s)} \to P_1K^* \to P_1K\pi$, $D_{(s)} \to P_1\phi \to P_1K\bar{K}$, and $D_{(s)} \to P_1\omega \to P_1K\bar{K}$, respectively. Each table is further categorized into three decay modes: Cabibbo-favored (CF), singly Cabibbo-suppressed (SCS), and doubly Cabibbo-suppressed (DCS) modes. The tables additionally specify the intermediate resonance decays and topological contributions, with symbols such as $T_{PV,PV}, C_{PV,PV}, E, A$ denoting these contributions to facilitate the analysis of branching fraction hierarchies. In the subsequent discussions, we analyze each table in turn. For our results in the FAT approach, the first uncertainty arises from the nonperturbative parameters in Eq. (20), while the second and third uncertainties are estimated by varying the form factors by 10% and unmeasured decay constants by 5%, respectively. Notably, the dominant source of uncertainty stems from the form factors. In the last column, we list the experimental data for comparison, while for unmeasured cases, the predictions of branching fractions can be tested against future experimental data.

A. Branching fractions of $D_{(s)} \to P_1(\rho \to)\pi\pi$ and $D_{(s)} \to P_1(K^* \to)K\pi$

The branching fractions of $D_{(s)} \to P_1(\rho \to)\pi\pi$ and $D_{(s)} \to P_1(K^* \to)K\pi$ are listed in Tables IV and V, respectively. In Table V, we specifically list quasi-two-body decays $D_{(s)} \to P_1K^* \to P_1K\pi$ mediated by the strong decays $K^{*0} \to K^+\pi^-$, $\bar{K}^{*0} \to K^-\pi^+$, and $K^{*-} \to K^-\pi^0$, where the K^* resonances involve contributions from $u\bar{u}$ sea quark pairs. For decays proceeding via $d\bar{d}$ sea quark pairs, such as $K^{*0} \to K^0\pi^0$, $\bar{K}^{*0} \to \bar{K}^0\pi^0$, and $K^{*-} \to \bar{K}^0\pi^-$, the corresponding branching ratios for $D_{(s)} \to P_1K^* \to P_1K\pi$ can be derived using the narrow-width approximation and are calculated by applying isospin conservation in the strong interaction dynamics of $K^* \to K\pi$ decay. The relations between branching ratios are explicitly expressed as

$$\mathcal{B}(\bar{K}^{*0} \to K^-\pi^+) = 2\mathcal{B}(\bar{K}^{*0} \to \bar{K}^0\pi^0), \tag{21}$$

$$\mathcal{B}(K^{*-} \to \bar{K}^0\pi^-) = 2\mathcal{B}(K^{*-} \to K^-\pi^0). \tag{22}$$

The observed hierarchies in the branching fractions of $D_{(s)} \to P_1(\rho \to)\pi\pi$ and $D_{(s)} \to P_1(K^* \to)K\pi$ decays arise from two key factors: one is the CKM hierarchy. CF decays ($V_{cs}^*V_{ud}$) dominate due to large CKM elements ($|V_{cs}| \sim 0.97, |V_{ud}| \sim 0.97$), leading to branching fractions about 10^{-3}–10^{-2}. SCS decays ($V_{cd(s)}^*V_{ud(s)}$) are suppressed by $|V_{cd}/V_{cs}|^2 \sim \lambda^2 \sim 0.05$, reducing branching fractions to 10^{-4}–10^{-3}. DCS decays ($V_{cd}^*V_{us}$) suffer an additional suppression $|V_{us}/V_{ud}|^2 \sim \lambda^2$, resulting in $\mathcal{B} \sim 10^{-5}$–10^{-4}. Another is topological diagram hierarchy. The relative strengths of diagrams follow $T_{VP/PV} > C_{VP/PV} > E > A$. This effect explains the observed hierarchies within the same type of CKM transition (e.g., CF, SCS, or DCS). For example, the branching fraction of $D_s^+ \to \pi^+(K^{*0} \to)K^+\pi^-$ (SCS, T_{VP} dominant) is larger than $D_s^+ \to \pi^0(K^{*+} \to)K^+\pi^0$ (SCS, C_{VP} dominant).

Nearly all CF and SCS modes of $D_{(s)} \to P_1(K^* \to)K\pi$, as well as several DCS modes, have already been experimentally measured, as indicated in the last column of Table V from PDG [96]. To compare with experimental results of some modes, we apply the approximate relation $\Gamma(\bar{K}^0) = 2\Gamma(\bar{K}_S^0)$ to convert $\bar{K}^0$ into the experimentally measurable K_S^0 component. Our theoretical predictions for $D_{(s)} \to P_1(K^* \to)K\pi$ agree well with experimental data. Other modes with comparable branching ratio, such as SCS modes $D^+ \to \bar{K}^0(K^{*+} \to)K^+\pi^0$, $D^+ \to \bar{K}^0(K^{*+} \to)K^+\pi^0$ and CF and SCS D_s decays, are also experimentally accessible.

For the branching fractions of $D_{(s)} \to P_1(\rho \to)\pi\pi$, we list the results of measured branching ratios of two-body decays of $D_{(s)} \to P_1\rho$ for comparison, as $\mathcal{B}(\rho \to \pi\pi) \sim 100\%$. Most of our results for quasi-two-body decay $D_{(s)} \to P_1\rho \to P_1\pi\pi$ are slightly smaller than those of the direct two-body decays $D_{(s)} \to P_1\rho$. The difference can be attributed to the relatively broad resonance width Γ_ρ of the $\rho(770)$ meson, which invalidates the narrow-width approximation typically used to factorize decay amplitudes. The $\rho(770)$ resonance dominates the $D^0 \to \pi^+\pi^-\pi^0$ decays, as evidenced by *BABAR*'s Dalitz analysis, where the fit fractions of $D^0 \to \pi^+(\rho^- \to)\pi^-\pi^0$, $D^0 \to \pi^-(\rho^+ \to)\pi^+\pi^0$, and $D^0 \to \pi^0(\rho^0 \to)\pi^+\pi^-$ are

$34.6 \pm 0.8 \pm 0.3$, $67.8 \pm 0.0 \pm 0.6$, and $26.2 \pm 0.5 \pm 1.1$, respectively [115]. Our results in the FAT approach, incorporating updated experimental data, yield smaller branching ratios than those derived from topological diagram methods [43], yet show closer agreement with the corresponding two-body decays of $D^0 \to \pi^+\rho^-$, $D^0 \to \pi^-\rho^+$, and $D^0 \to \pi^0\rho^0$. This improved consistency suggests that the FAT framework better accounts for nonfactorizable effects (e.g., final-state interactions and resonance interference) and flavor $SU(3)$ asymmetry in the quasi-two-body decay formalism. The latter arises from mass differences between u, d, and s quarks and dynamical asymmetries in decay amplitudes, which are not fully captured by topological diagram approaches relying on exact SU(3) symmetry assumptions.

As shown in Tables IV and V, the $D_{(s)} \to K\pi\pi$ decays can proceed via contributions from both ρ and K^* resonances. For example, $D^0 \to K^+\pi^-\pi^0$ receives contributions from ρ^-, K^{*+}, and K^{*0} resonances. $D^+ \to K^+\pi^+\pi^-$ is mediated by ρ^0 and K^{*0} resonances. $D_s^+ \to K^+\pi^+\pi^-$ similarly involves ρ^0 and K^{*0} resonances. In this work, we focus on calculating the branching ratios for these decay modes. The analysis of CP asymmetries, arising from interference effects between overlapping resonances (e.g., $\rho - K^*$ interference in phase space), will be addressed in future work. Such interference phenomena are critical for understanding dynamics in three-body decays but require a detailed amplitude analysis of the Dalitz plot.

B. Branching fractions of $D_{(s)} \to P_1\phi \to P_1K\bar{K}$

We present the branching fraction results of $D_{(s)} \to P_1(\phi \to)K\bar{K}$ decays in Table VI alongside corresponding PDG values [96] in the last column. The branching ratios of $D_{(s)} \to \pi, K(\phi \to)K\bar{K}$ have been measured by experiments and the results in the FAT approach agree well with these experimental data. In addition to listing the quasi-two-body decay modes involving $u\bar{u}$ sea quarks in $\phi \to K^+K^-$, we also include those with $d\bar{d}$ sea quarks in $\phi \to K^0\bar{K}^0$. By summing contributions from $D_{(s)} \to P_1(\phi \to)K^+K^-$ and $D_{(s)} \to P_1(\phi \to)K^0\bar{K}^0$ decays (which share the same weak transition but different strong decay), we recover the corresponding two-body decay $D \to P_1\phi$ branching fractions through the narrow-width approximation. For instance, the sum of our predictions for the unmeasured quasi-two-body decays $D^0 \to \eta(\phi \to)K^+K^-$ and $D^0 \to \eta(\phi \to)K^0\bar{K}^0$ is in agreement with the PDG value for the two-body decay $\mathcal{B}(D^0 \to \eta\phi) = (0.184 \pm 0.012) \times 10^{-4}$.

TABLE IV. Branching Fractions in the FAT approach of quasi-two-body decays $D_{(s)} \to P_1(\rho \to)\pi\pi$ ($\times 10^{-3}$), (with the uncertainties from the fitted parameters, form factors and decay constants, respectively,) together with the experimental data [96]. In the second column, the characters $T_{PV,PV}, C_{PV,PV}, E, A$ represent the corresponding topological diagram contributions.

Modes	Amplitudes	FAT results	Experimental data
CF	$V_{cs}^* V_{ud}$		
$D^0 \to K^-(\rho^+ \to)\pi^+\pi^0$	T_{PV}, E	$89.78 \pm 4.14 \pm 21.12 \pm 9.08$	112 ± 7
$D^0 \to \bar{K}^0(\rho^0 \to)\pi^+\pi^-$	C_{VP}, E	$9.30 \pm 1.17 \pm 2.30 \pm 0.32$	12.6 ± 1.6
$D^+ \to \bar{K}^0(\rho^+ \to)\pi^+\pi^0$	T_{PV}, C_{VP}	$90.61 \pm 9.51 \pm 36.00 \pm 16.42$	122.8 ± 12
$D^+ \to \eta(\rho^+ \to)\pi^+\pi^0$	T_{PV}, C_{VP}, A	$0.18 \pm 0.14 \pm 0.13 \pm 0.04$	
$D^+ \to \eta'(\rho^+ \to)\pi^+\pi^0$	T_{PV}, C_{VP}, A	$1.68 \pm 0.05 \pm 0.23 \pm 0.10$	
$D_s^+ \to \eta(\rho^+ \to)\pi^+\pi^0$	T_{PV}, A	$79.21 \pm 3.34 \pm 16.63 \pm 7.92$	89 ± 8
$D_s^+ \to \eta'(\rho^+ \to)\pi^+\pi^0$	T_{PV}, A	$34.66 \pm 0.98 \pm 6.59 \pm 3.46$	58 ± 15
SCS	$V_{cd(s)}^* V_{ud(s)}$		
$D^0 \to \pi^+(\rho^- \to)\pi^-\pi^0$	T_{VP}, E	$4.37 \pm 0.30 \pm 0.72 \pm 0.11$	5.15 ± 0.25
$D^0 \to \pi^-(\rho^+ \to)\pi^+\pi^0$	T_{PV}, E	$8.55 \pm 0.44 \pm 1.50 \pm 0.86$	10.1 ± 0.4
$D^0 \to \pi^0(\rho^0 \to)\pi^+\pi^-$	$C_{PV,VP}, E$	$2.65 \pm 0.24 \pm 0.30 \pm 0.18$	3.86 ± 0.23
$D^0 \to \eta(\rho^0 \to)\pi^+\pi^-$	$C_{PV,VP}, E$	$0.42 \pm 0.10 \pm 0.08 \pm 0.00$	
$D^0 \to \eta'(\rho^0 \to)\pi^+\pi^-$	$C_{PV,VP}, E$	$0.24 \pm 0.01 \pm 0.03 \pm 0.01$	
$D^+ \to \pi^+(\rho^0 \to)\pi^+\pi^-$	T_{VP}, C_{PV}, A	$0.48 \pm 0.04 \pm 0.14 \pm 0.02$	0.83 ± 0.14
$D^+ \to \pi^0(\rho^+ \to)\pi^+\pi^0$	T_{PV}, C_{VP}, A	$2.90 \pm 0.24 \pm 1.05 \pm 0.49$	
$D_s^+ \to K^+(\rho^0 \to)\pi^+\pi^-$	C_{PV}, A	$1.59 \pm 0.10 \pm 0.32 \pm 0.16$	2.17 ± 0.25
$D_s^+ \to K^0(\rho^+ \to)\pi^+\pi^0$	T_{PV}, A	$8.16 \pm 0.29 \pm 1.70 \pm 0.82$	5.46 ± 0.95
DCS	$V_{cd}^* V_{us}$		
$D^0 \to K^+(\rho^- \to)\pi^-\pi^0$	T_{VP}, E	$0.12 \pm 0.01 \pm 0.03 \pm 0.00$	
$D^0 \to K^0(\rho^0 \to)\pi^+\pi^-$	C_{VP}, E	$0.03 \pm 0.00 \pm 0.01 \pm 0.00$	
$D^+ \to K^+(\rho^0 \to)\pi^+\pi^-$	T_{VP}, A	$0.23 \pm 0.01 \pm 0.05 \pm 0.00$	0.19 ± 0.05
$D^+ \to K^0(\rho^+ \to)\pi^+\pi^0$	C_{VP}, A	$0.19 \pm 0.02 \pm 0.04 \pm 0.00$	

TABLE V. Same as Table IV for quasi-two-body decays $D_{(s)} \to P_1(K^* \to)K\pi$ in units of 10^{-3}.

Decay modes	Amplitudes	FAT results	Experimental data
CF	$V_{cs}^* V_{ud}$		
$D^0 \to \pi^+(K^{*-} \to)K^-\pi^0$	T_{VP}, E	$18.84 \pm 1.43 \pm 3.00 \pm 0.52$	19.5 ± 2.4
$D^0 \to \pi^0(\bar{K}^{*0} \to)K_S^0\pi^0$	C_{PV}, E	$5.67 \pm 0.50 \pm 0.98 \pm 0.57$	8.1 ± 0.7
$D^0 \to \eta(\bar{K}^{*0} \to)K_S^0\pi^0$	C_{PV}, E	$3.01 \pm 0.34 \pm 0.60 \pm 0.30$	2.9 ± 0.7
$D^+ \to \pi^+(\bar{K}^{*0} \to)K^-\pi^+$	T_{VP}, C_{PV}	$11.17 \pm 0.92 \pm 3.49 \pm 1.72$	10.4 ± 1.2
$D_s^+ \to K^+(\bar{K}^{*0} \to)K^-\pi^+$	C_{PV}, A	$25.00 \pm 1.64 \pm 6.73 \pm 2.65$	25.8 ± 0.6
$D_s^+ \to \bar{K}^0(K^{*+} \to)K^+\pi^0$	C_{VP}, A	$5.22 \pm 0.73 \pm 1.26 \pm 0.16$	
SCS	$V_{cd(s)}^* V_{ud(s)}$		
$D^0 \to K^+(K^{*-} \to)K^-\pi^0$	T_{VP}, E	$0.40 \pm 0.03 \pm 0.10 \pm 0.02$	0.54 ± 0.04
$D^0 \to K^-(K^{*+} \to)K^+\pi^0$	T_{PV}, E	$1.53 \pm 0.06 \pm 0.35 \pm 0.15$	1.52 ± 0.07
$D^0 \to K_S^0(\bar{K}^{*0} \to)K^-\pi^+$	E	$0.12 \pm 0.03 \pm 0.00 \pm 0.02$	0.08 ± 0.02
$D^0 \to \bar{K}_S^0(K^{*0} \to)K^+\pi^-$	E	$0.12 \pm 0.03 \pm 0.00 \pm 0.02$	0.11 ± 0.02
$D^+ \to K^+(\bar{K}^{*0} \to)K^-\pi^+$	T_{VP}, A	$2.60 \pm 0.13 \pm 0.62 \pm 0.08$	$2.49^{+0.08}_{-0.13}$
$D^+ \to \bar{K}^0(K^{*+} \to)K^+\pi^0$	T_{PV}, A	$4.26 \pm 0.12 \pm 0.94 \pm 0.42$	
$D_s^+ \to \pi^+(K^{*0} \to)K^+\pi^-$	T_{VP}, A	$1.56 \pm 0.10 \pm 0.34 \pm 0.03$	1.40 ± 0.24
$D_s^+ \to \pi^0(K^{*+} \to)K^+\pi^0$	C_{VP}, A	$0.16 \pm 0.02 \pm 0.03 \pm 0.00$	
$D_s^+ \to \eta(K^{*+} \to)K^+\pi^0$	T_{PV}, C_{VP}, A	$0.47 \pm 0.08 \pm 0.16 \pm 0.08$	
$D_s^+ \to \eta'(K^{*+} \to)K^+\pi^0$	T_{PV}, C_{VP}, A	$0.19 \pm 0.01 \pm 0.05 \pm 0.03$	
DCS	$V_{cd}^* V_{us}$		
$D^0 \to \pi^-(K^{*+} \to)K_S^0\pi^+$	T_{VP}, E	$0.15 \pm 0.01 \pm 0.03 \pm 0.02$	$0.11^{+0.06}_{-0.03}$
$D^0 \to \pi^0(K^{*0} \to)K^+\pi^-$	C_{PV}, E	$0.06 \pm 0.01 \pm 0.01 \pm 0.01$	
$D^0 \to \eta(K^{*0} \to)K^+\pi^-$	C_{PV}, E	$0.02 \pm 0.00 \pm 0.00 \pm 0.00$	
$D^+ \to \pi^0(K^{*+} \to)K^+\pi^0$	T_{PV}, A	$0.14 \pm 0.00 \pm 0.03 \pm 0.01$	
$D^+ \to \pi^+(K^{*0} \to)K^+\pi^-$	C_{PV}, A	$0.21 \pm 0.01 \pm 0.05 \pm 0.02$	0.23 ± 0.04
$D^+ \to \eta(K^{*+} \to)K^+\pi^0$	T_{PV}, A	$0.06 \pm 0.00 \pm 0.01 \pm 0.01$	
$D_s^+ \to K^+(K^{*0} \to)K^+\pi^-$	T_{VP}, C_{PV}	$0.02 \pm 0.00 \pm 0.00 \pm 0.00$	0.06 ± 0.03
$D_s^+ \to K^0(K^{*+} \to)K^+\pi^0$	T_{PV}, C_{VP}	$0.06 \pm 0.00 \pm 0.02 \pm 0.01$	

TABLE VI. Same as Table IV for quasi-two-body decays $D_{(s)} \to P_1(\phi \to)KK$ in units of 10^{-3}.

Decay modes	Amplitudes	FAT results	Experiment
CF	$V_{cs}^* V_{ud}$		
$D^0 \to K_S^0(\phi \to)K^+K^-$	E	$1.62 \pm 0.16 \pm 0 \pm 0.23$	2.03 ± 0.15
$\to \bar{K}^0(\phi \to)K^0\bar{K}^0$		$2.20 \pm 0.22 \pm 0 \pm 0.31$	
$D_s^+ \to \pi^+(\phi \to)K^+K^-$	T_{VP}	$23.94 \pm 0.14 \pm 1.53 \pm 0.02$	22.2 ± 0.6
$\to \pi^+(\phi \to)K^0\bar{K}^0$		$16.31 \pm 0.10 \pm 1.16 \pm 0.02$	
SCS	$V_{cd(s)}^* V_{ud(s)}$		
$D^0 \to \pi^0(\phi \to)K^+K^-$	C_{PV}	$0.62 \pm 0.01 \pm 0.07 \pm 0.03$	0.66 ± 0.04
$\to \pi^0(\phi \to)K^0\bar{K}^0$		$0.43 \pm 0.01 \pm 0.04 \pm 0.02$	
$D^0 \to \eta(\phi \to)K^+K^-$	C_{PV}, E	$0.13 \pm 0.03 \pm 0 \pm 0.02$	
$\to \eta(\phi \to)K^0\bar{K}^0$		$0.09 \pm 0.02 \pm 0 \pm 0.01$	
$D^+ \to \pi^+(\phi \to)K^+K^-$	C_{PV}	$3.18 \pm 0.06 \pm 0.34 \pm 0.17$	$2.69^{+0.07}_{-0.08}$
$\to \pi^+(\phi \to)K^0\bar{K}^0$		$2.18 \pm 0.03 \pm 0.18 \pm 0.09$	
$D_s^+ \to K^+(\phi \to)K^+K^-$	T_{VP}, C_{PV}, A	$0.13 \pm 0.03 \pm 0.06 \pm 0.01$	0.088 ± 0.02
$\to K^+(\phi \to)K^0\bar{K}^0$		$0.09 \pm 0.02 \pm 0.04 \pm 0.01$	
DCS	$V_{cd}^* V_{us}$		
$D^0 \to K^0(\phi \to)K^+K^-$	E	$0.009 \pm 0.001 \pm 0 \pm 0.001$	
$\to K^0(\phi \to)K^0\bar{K}^0$		$0.006 \pm 0.001 \pm 0 \pm 0.001$	
$D^+ \to K^+(\phi \to)K^+K^-$	A	$(3.7 \pm 0.6 \pm 0 \pm 0.5) \times 10^{-3}$	$(4.4 \pm 0.6) \times 10^{-3}$
$\to K^+(\phi \to)K^0\bar{K}^0$		$(2.5 \pm 0.4 \pm 0 \pm 0.4) \times 10^{-3}$	

TABLE VII. The virtual effects of $D_{(s)} \to P_1(\omega \to)K\bar{K}$ decays, which happen when the pole masses of ω are smaller than the invariant mass of $K\bar{K}$.

Decay modes	Amplitudes	FAT results
CF	$V_{cs}^* V_{ud}$	
$D^0 \to \bar{K}^0(\omega \to)K^+K^-$	C_{VP}, E	$(0.90 \pm 0.07 \pm 0.13 \pm 0.03) \times 10^{-5}$
$D_s^+ \to \pi^+(\omega \to)K^+K^-$	A	$(3.28 \pm 0.22 \pm 0 \pm 0.43) \times 10^{-6}$
SCS	$V_{cd(s)}^* V_{ud(s)}$	
$D^0 \to \pi^0(\omega \to)K^+K^-$	C_{PV}, C_{VP}, E	$(7.11 \pm 1.42 \pm 1.99 \pm 1.11) \times 10^{-7}$
$D^0 \to \eta(\omega \to)K^+K^-$	C_{PV}, C_{VP}, E	$(1.05 \pm 0.06 \pm 0.13 \pm 0.05) \times 10^{-6}$
$D^+ \to \pi^+(\omega \to)K^+K^-$	T_{VP}, C_{PV}, A	$(5.49 \pm 0.84 \pm 2.65 \pm 1.07) \times 10^{-7}$
$D_s^+ \to K^+(\omega \to)K^+K^-$	C_{PV}, A	$(1.86 \pm 0.09 \pm 0.35 \pm 0.19) \times 10^{-6}$
DCS	$V_{cd}^* V_{us}$	
$D^0 \to K^0(\omega \to)K^+K^-$	C_{VP}, E	$(2.56 \pm 0.20 \pm 0.38 \pm 0.09) \times 10^{-8}$
$D^+ \to K^+(\omega \to)K^+K^-$	T_{VP}, A	$(9.69 \pm 0.31 \pm 1.82 \pm 0.11) \times 10^{-8}$

C. The virtual effects of $D_{(s)} \to P_1(\omega \to)K\bar{K}$

The decay modes $D_{(s)} \to P_1(\omega \to)K\bar{K}$ denote a distinct category of processes where the ω resonance pole mass ($m_\omega \approx 783$ MeV) lies below the $K\bar{K}$ production threshold (~987 MeV for K^+K^- and ~994 MeV for $K^0\bar{K}^0$). These decays proceed via virtual transitions [the Breit-Wigner-tail (BWT) effect], a mechanism previously studied in B-meson decays on the theoretical side [81–83] and by experiments in Belle [116] and LHCb [117]. The BWT effects play an important role in probing the shape function of vector resonances and analyzing the dynamics of three-body decay mechanisms. In Table VII, we quantify these virtual effects using the FAT approach. Predicted branching fractions for most modes lie in the range 10^{-7}–10^{-6}, rendering them experimentally inaccessible with current precision. However, CF modes approaching 10^{-5} may warrant experimental analysis. We exclusively consider the subprocesses $\omega \to K^+K^-$ in our analysis. The omission of $\omega \to K^0\bar{K}^0$ is justified by the negligible phase space difference between K^+K^- and $K^0\bar{K}^0$ final states (stemming from the small $K^0 - K^+$ mass difference, $\Delta_{m_K} \approx 4$ MeV), which results in virtually identical BWT behaviors. The Breit-Wigner propagators in Eq. (5) exhibit specific kinematics in these decays: For the invariant mass square $s \geq 1$ GeV^2 (for above the ω pole), the imaginary term $im_\omega\Gamma_\omega(s)$ becomes subdominant. Consequently, virtual contributions show minimal sensitivity to the ω meson's full decay width $\Gamma_\omega(s)$, as the propagator behavior is governed by the $(m_\omega^2 - s)$ denominator term.

IV. CONCLUSION

Theoretical studies of charm meson decays remain limited due to the intermediate mass scale of the charm meson, which lies between perturbative and nonperturbative regimes. This gap is particularly pronounced for three-body D-meson decays, despite recent measurements of such decays with resonance contributions by BESIII and other experiments. In this work, we systematically investigate the quasi-two-body decays $D_{(s)} \to P_1(V \to)P_2P_3$, where V denotes intermediate vector resonances (ρ, K^*, ω, ϕ), decaying strongly to pseudoscalars P_2 and P_3. These processes originate from $c \to d/s$ transitions forming P_1V intermediate states. Using the FAT approach, we can describe well the nonperturbative contributions for the intermediate two-body decays $D_{(s)} \to P_1V$. The subsequent resonant dynamics are modeled via the relativistic RBW line shape, consistent with experimental analyses. We categorize the decays into four types based on the vector resonance: $D_{(s)} \to P_1(\rho \to)\pi\pi$, $D_{(s)} \to P_1(K^* \to)K\pi$, $D_{(s)} \to P_1(\phi \to)KK$, and $D_{(s)} \to P_1(\omega \to)KK$. The first three classes are governed by pole dynamics, while the ω-mediated channel arises predominantly from the BWT interference effect. This systematic framework bridges theoretical predictions with experimental resonance analyses in three-body D-meson decays.

In this work, we calculate the branching ratios for the four categories of quasi-two-body decay modes. Utilizing updated nonperturbative parameters derived from a global fit to precise experimental data, our results are in alignment with existing measurements. The theoretical uncertainties in our approach are small, owing to the precise determination of nonfactorizable parameters from data-driven analyses. For unmeasured modes, we predict their branching ratios and are waiting for future experiments to test, especially for those on the order of 10^{-4}–10^{-3}, which are promising candidates for future observation in high-precision experiments like BESIII and LHCb. Notably, the fourth category decay $D_{(s)} \to P_1(\omega \to)KK$ proceeds via the tail effects of the ω resonance in the KK channel. This mechanism provides an opportunity to probe the shape function of vector resonances, offering insights into the interplay between resonance dynamics and three-body decay mechanisms.

ACKNOWLEDGMENTS

The work is supported by the National Natural Science Foundation of China under Grant No. 12465017.

DATA AVAILABILITY

The data that support the findings of this article are openly available [96].

[1] M. Ablikim *et al.* (BESIII Collaboration), Measurements of the branching fractions for $D^+ \to K_S^0 K_S^0 K^+$, $K_S^0 K_S^0 \pi^+$ and $D^0 \to K_S^0 K_S^0$, $K_S^0 K_S^0 K_S^0$, Phys. Lett. B **765**, 231 (2017).

[2] M. Ablikim *et al.* (BESIII Collaboration), Measurement of singly Cabibbo-suppressed decays $D^0 \to \pi^0\pi^0\pi^0$, $\pi^0\pi^0\eta$, $\pi^0\eta\eta$ and $\eta\eta\eta$, Phys. Lett. B **781**, 368 (2018).

[3] M. Ablikim *et al.* (BESIII Collaboration), Observation of $D^{0(+)} \to K_S^0 \pi^{0(+)}\eta'$ and improved measurement of $D^0 \to K^-\pi^+\eta'$, Phys. Rev. D **98**, 092009 (2018).

[4] M. Ablikim *et al.* (BESIII Collaboration), Measurements of the absolute branching fractions and CP asymmetries for $D^+ \to K_{S,L}^0 K^+(\pi^0)$, Phys. Rev. D **99**, 032002 (2019).

[5] M. Ablikim *et al.* (BESIII Collaboration), Observation of $D^+ \to \eta\eta\pi^+$ and improved measurement of $D^{0(+)} \to \eta\pi^+\pi^{-(0)}$, Phys. Rev. D **101**, 052009 (2020).

[6] M. Ablikim *et al.* (BESIII Collaboration), Amplitude analysis of $D_s^+ \to \pi^+\pi^-\pi^+$, Phys. Rev. D **106**, 112006 (2022).

[7] R. Aaij *et al.* (LHCb Collaboration), Search for CP violation in $D^+ \to K^-K^+\pi^+$ decays, Phys. Rev. D **84**, 112008 (2011).

[8] R. Aaij *et al.* (LHCb Collaboration), Search for CP violation in the decay $D^+ \to \pi^-\pi^+\pi^+$, Phys. Lett. B **728**, 585 (2014).

[9] R. Aaij *et al.* (LHCb Collaboration), Search for CP violation in $D^0 \to \pi^?\pi^+\pi^0$ decays with the energy test, Phys. Lett. B **740**, 158 (2015).

[10] R. Aaij *et al.* (LHCb Collaboration), Search for CP violation in $D_{(s)}^+ \to K^-K^+K^+$ decays, J. High Energy Phys. 07 (2023) 067.

[11] R. Aaij *et al.* (LHCb Collaboration), Measurement of CP violation observables in $D^+ \to K^-K^+\pi^+$ decays, Phys. Rev. Lett. **133**, 251801 (2024).

[12] S. Kopp *et al.* (CLEO Collaboration), Dalitz analysis of the decay $D^0 \to K^-\pi^+\pi^0$, Phys. Rev. D **63**, 092001 (2001).

[13] S. Dobbs *et al.* (CLEO Collaboration), Measurement of absolute hadronic branching fractions of D mesons and $e^+e^- \to D\bar{D}$ cross-sections at the $\psi(3770)$, Phys. Rev. D **76**, 112001 (2007).

[14] P. Rubin *et al.* (CLEO Collaboration), Search for CP violation in the Dalitz-Plot analysis of $D^\pm \to K^+K^-\pi^\pm$, Phys. Rev. D **78**, 072003 (2008).

[15] R. A. Briere *et al.* (CLEO Collaboration), Analysis of $D^+ \to K^-\pi^+e^+\nu_e$ and $D^+ \to K^-\pi^+\mu^+\nu_\mu$ semileptonic decays, Phys. Rev. D **81**, 112001 (2010).

[16] N. Lowrey *et al.* (CLEO Collaboration), Analysis of the decay $D^0 \to K_S^0\pi^0\pi^0$, Phys. Rev. D **84**, 092005 (2011).

[17] J. Insler *et al.* (CLEO Collaboration), Studies of the decays $D^0 \to K_S^0 K^-\pi^+$ and $D^0 \to K_S^0 K^+\pi^-$, Phys. Rev. D **85**, 092016 (2012); **94**, 099905(E) (2016).

[18] P. U. E. Onyisi *et al.* (CLEO Collaboration), Improved measurement of absolute hadronic branching fractions of the D_s^+ meson, Phys. Rev. D **88**, 032009 (2013).

[19] G. Bonvicini *et al.* (CLEO Collaboration), Updated measurements of absolute D^+ and D^0 hadronic branching fractions and $\sigma(e^+e^- \to D\bar{D})$ at $E_{\rm cm} = 3774$ MeV, Phys. Rev. D **89**, 072002 (2014); **91**, 019903(E) (2015).

[20] K. Arinstein *et al.* (Belle Collaboration), Measurement of the ratio $B(D^0 \to \pi^+\pi^-\pi^0)/B(D^0 \to K^-\pi^+\pi^0)$ and the time-integrated CP asymmetry in $D^0 \to \pi^+\pi^-\pi^0$, Phys. Lett. B **662**, 102 (2008).

[21] I. Adachi *et al.* (Belle-II and Belle Collaboration), Model-independent measurement of D^0-$\bar{D}^0$ mixing parameters in $D^0 \to K_S^0\pi^+\pi^-$ decays at Belle and Belle II, arXiv: 2410.22961.

[22] B. Aubert *et al.* (*BABAR* Collaboration), Measurement of γ in $B^\mp \to D^{(*)}K^\mp$ decays with a Dalitz analysis of $D \to K_S^0\pi^-\pi^+$, Phys. Rev. Lett. **95**, 121802 (2005).

[23] B. Aubert *et al.* (*BABAR* Collaboration), Precise branching ratio measurements of the decays $D^0 \to \pi^-\pi^+\pi^0$ and $D^0 \to K^-K^+\pi^0$, Phys. Rev. D **74**, 091102 (2006).

[24] B. Aubert *et al.* (*BABAR* Collaboration), Search for CP violation in neutral D meson Cabibbo-suppressed three-body decays, Phys. Rev. D **78**, 051102 (2008).

[25] B. Aubert *et al.* (*BABAR* Collaboration), Dalitz plot analysis of $D_s^+ \to \pi^+\pi^-\pi^+$, Phys. Rev. D **79**, 032003 (2009).

[26] J. P. Lees *et al.* (*BABAR* Collaboration), Search for direct CP violation in singly Cabibbo-suppressed $D^\pm \to K^+K^-\pi^\pm$ decays, Phys. Rev. D **87**, 052010 (2013).

[27] A. J. Buras, J. M. Gerard, and R. Ruckl, 1/n expansion for exclusive and inclusive charm decays, Nucl. Phys. **B268**, 16 (1986).

[28] B. Aubert *et al.* (*BABAR* Collaboration), Amplitude analysis of the decay $D^0 \to K^-K^+\pi^0$, Phys. Rev. D **76**, 011102 (2007).

[29] M. Beneke, G. Buchalla, M. Neubert, and C. T. Sachrajda, QCD factorization for exclusive, nonleptonic B meson decays: General arguments and the case of heavy light final states, Nucl. Phys. **B591**, 313 (2000).

[30] C.-D. Lu, K. Ukai, and M.-Z. Yang, Branching ratio and CP violation of $\vec{B}\pi\pi$ decays in perturbative QCD approach, Phys. Rev. D **63**, 074009 (2001).

[31] Y. Y. Keum, H.-N. Li, and A. I. Sanda, Penguin enhancement and $B \to K\pi$ decays in perturbative QCD, Phys. Rev. D **63**, 054008 (2001).

[32] A. Ryd and A. A. Petrov, Hadronic D and D_s meson decays, Rev. Mod. Phys. **84**, 65 (2012).

[33] B. Bhattacharya and J. L. Rosner, Decays of charmed mesons to PV final states, Phys. Rev. D **79**, 034016 (2009); **81**, 099903(E) (2010).

[34] W.-F. Wang, Subprocesses $\rho(770, 1450) \to K\bar{K}$ for the three-body hadronic D meson decays, Phys. Rev. D **104**, 116019 (2021).

[35] J. Brod, A. L. Kagan, and J. Zupan, Size of direct CP violation in singly Cabibbo-suppressed D decays, Phys. Rev. D **86**, 014023 (2012).

[36] H.-Y. Cheng and C.-W. Chiang, Two-body hadronic charmed meson decays, Phys. Rev. D **81**, 074021 (2010).

[37] H.-Y. Cheng and C.-W. Chiang, Direct CP violation in two-body hadronic charmed meson decays, Phys. Rev. D **85**, 034036 (2012); **85**, 079903(E) (2012).

[38] H.-Y. Cheng and C.-W. Chiang, $SU(3)$ symmetry breaking and CP violation in D → PP decays, Phys. Rev. D **86**, 014014 (2012).

[39] C.-H. Chen, C.-Q. Geng, and W. Wang, CP violation in $D^0 \to (K^-K^+, \pi^-\pi^+)$ from diquarks, Phys. Rev. D **85**, 077702 (2012).

[40] H.-Y. Cheng, C.-W. Chiang, and A.-L. Kuo, Global analysis of two-body D → VP decays within the framework of flavor symmetry, Phys. Rev. D **93**, 114010 (2016).

[41] H.-Y. Cheng and C.-W. Chiang, Revisiting CP violation in $D \to PP$ and VP decays, Phys. Rev. D **100**, 093002 (2019).

[42] Y.-K. Hsiao, Y. Yu, and B.-C. Ke, Resonant $a_0(980)$ state in triangle rescattering $D_s^+ \to \pi^+\pi^0\eta$ decays, Eur. Phys. J. C **80**, 895 (2020).

[43] H.-Y. Cheng and C.-W. Chiang, CP violation in quasi-two-body D → VP decays and three-body D decays mediated by vector resonances, Phys. Rev. D **104**, 073003 (2021).

[44] H.-n. Li, C.-D. Lu, and F.-S. Yu, Branching ratios and direct CP asymmetries in $D \to PP$ decays, Phys. Rev. D **86**, 036012 (2012).

[45] Q. Qin, H.-n. Li, C.-D. Lü, and F.-S. Yu, Branching ratios and direct CP asymmetries in $D \to PV$ decays, Phys. Rev. D **89**, 054006 (2014).

[46] Q. Qin, C. Wang, D. Wang, and S.-H. Zhou, The factorization-assisted topological-amplitude approach and its applications, Front. Phys. (Beijing) **18**, 64602 (2023).

[47] H. Zhou, B. Zheng, and Z.-H. Zhang, Analysis of CP violation in $D^0 \to K^+K^-\pi^0$, Adv. High Energy Phys. **2018**, 7627308 (2018).

[48] W.-F. Wang, J.-Y. Xu, S.-H. Zhou, and P.-P. Shi, Contributions of $\rho(770, 1450) \to \omega\pi$ for the Cabibbo-favored $D \to h\omega\pi$ decays, arXiv:2502.11159.

[49] A. Dery, Y. Grossman, S. Schacht, and A. Soffer, Probing the $\Delta U = 0$ rule in three body charm decays, J. High Energy Phys. 05 (2021) 179.

[50] R. Molina, J.-J. Xie, W.-H. Liang, L.-S. Geng, and E. Oset, Theoretical interpretation of the $D_s^+ \to \pi^+\pi^0\eta$ decay and the nature of $a_0(980)$, Phys. Lett. B **803**, 135279 (2020).

[51] G. Toledo, N. Ikeno, and E. Oset, Theoretical study of the $D^0 \to K^-\pi^+\eta$ reaction, Eur. Phys. J. C **81**, 268 (2021).

[52] L. Roca and E. Oset, Scalar resonances in the $D^+ \to K^-K^+K^+$ decay, Phys. Rev. D **103**, 034020 (2021).

[53] L. R. Dai, E. Oset, and L. S. Geng, The $D_s^+ \to \pi^+K_S^0K_S^0$ reaction and the $I = 1$ partner of the $f_0(1710)$ state, Eur. Phys. J. C **82**, 225 (2022).

[54] L. R. Dai and E. Oset, Dynamical generation of the scalar $f_0(500)$, $f_0(980)$, and $K_0^*(700)$ resonances in the $D_s^+ \to K^+\pi^+\pi^-$ reaction, Phys. Rev. D **109**, 054008 (2024).

[55] M. Bayar, R. Molina, E. Oset, M.-Z. Liu, and L.-S. Geng, Subtleties in triangle loops for $D_s^+ \to \rho^+\eta \to \pi^+\pi^0\eta$ in $a_0(980)$ production, Phys. Rev. D **109**, 076027 (2024).

[56] N. Ikeno, J. M. Dias, W.-H. Liang, and E. Oset, $D^+ \to K_s^0\pi^+\eta$ reaction and $a_0(980)^+$, Eur. Phys. J. C **84**, 469 (2024).

[57] N. Ikeno, M. Bayar, and E. Oset, Combined theoretical study of the $D^+ \to \pi^+\eta\eta$ and $D^+ \to \pi^+\pi^0\eta$ reactions, Eur. Phys. J. C **81**, 377 (2021).

[58] D. Boito, J. P. Dedonder, B. El-Bennich, R. Escribano, R. Kaminski, L. Lesniak, and B. Loiseau, Parametrizations of three-body hadronic B- and D-decay amplitudes in terms of analytic and unitary meson-meson form factors, Phys. Rev. D **96**, 113003 (2017).

[59] P.-F. Guo, D. Wang, and F.-S. Yu, Strange axial-vector mesons in D meson decays, Nucl. Phys. Rev. **36**, 125 (2019).

[60] Y. Yu, Y.-K. Hsiao, and B.-C. Ke, Study of the $D_s^+ \to a_0(980)\rho$ and $a_0(980)\omega$ decays, Eur. Phys. J. C **81**, 1093 (2021).

[61] W.-J. Song, S.-Q. Wang, Q. Qin, and Y. Li, Cp violation analysis of $D^0 \to M^0K \to M^0(\pi^\pm\ell^\mp\nu)$, Eur. Phys. J. C **85**, 300 (2025).

[62] F. Niecknig and B. Kubis, Dispersion-theoretical analysis of the $D^+ \to K^-\pi^+\pi^+$ Dalitz plot, J. High Energy Phys. 10 (2015) 142.

[63] S. X. Nakamura, Coupled-channel analysis of $D^+ \to K^-\pi^+\pi^+$ decay, Phys. Rev. D **93**, 014005 (2016).

[64] P. C. Magalhaes, M. R. Robilotta, K. S. F. F. Guimaraes, T. Frederico, W. de Paula, I. Bediaga, A. C. d. Reis, C. M. Maekawa, and G. R. S. Zarnauskas, Towards three-body unitarity in $D^+ \to K^-\pi^+\pi^+$, Phys. Rev. D **84**, 094001 (2011).

[65] R. T. Aoude, P. C. Magalhães, A. C. Dos Reis, and M. R. Robilotta, Multimeson model for the $D^+ \to K^+K^-K^+$ decay amplitude, Phys. Rev. D **98**, 056021 (2018).

[66] H.-N. Li, H. Umeeda, F. Xu, and F.-S. Yu, D meson mixing as an inverse problem, Phys. Lett. B **810**, 135802 (2020).

[67] M. Saur and F.-S. Yu, Charm CPV: Observation and prospects, Sci. Bull. **65**, 1428 (2020).

[68] M. Ablikim *et al.* (BESIII Collaboration), Amplitude analysis of the $D^+ \to K_S^0\pi^+\pi^0$ Dalitz plot, Phys. Rev. D **89**, 052001 (2014).

[69] M. Ablikim *et al.* (BESIII Collaboration), Amplitude analysis and branching fraction measurement of the decay $D_s^+ \to K^+\pi^+\pi^-$, J. High Energy Phys. 08 (2022) 196.

[70] M. Ablikim *et al.* (BESIII Collaboration), Analysis of the decay $D^0 \to K_S^0K^+K^-$, arXiv:2006.02800.

[71] M. Ablikim *et al.* (BESIII Collaboration), Amplitude analysis and branching fraction measurement of $D_s^+ \to K^+K^-\pi^+$, Phys. Rev. D **104**, 012016 (2021).

[72] M. Ablikim *et al.* (BESIII Collaboration), Amplitude analysis and branching-fraction measurement of $D_s^+ \to K_S^0\pi^+\pi^0$, J. High Energy Phys. 06 (2021) 181.

[73] M. Ablikim *et al.* (BESIII Collaboration), Study of the decay $D^+ \to K^*(892)^+ K_S^0$ in $D^+ \to K^+ K_S^0 \pi^0$, Phys. Rev. D **104**, 012006 (2021).

[74] M. Ablikim *et al.* (BESIII Collaboration), Observation of the doubly Cabibbo-suppressed decays $D^+ \to K^+ \pi^0 \pi^0$ and $D^+ \to K^+ \pi^0 \eta$, J. High Energy Phys. 09 (2022) 107.

[75] M. Ablikim *et al.* (BESIII Collaboration), Amplitude analysis and branching-fraction measurement of $D_s^+ \to \pi^+ \pi^0 \eta'$, J. High Energy Phys. 04 (2022) 058.

[76] S.-H. Zhou, Y.-B. Wei, Q. Qin, Y. Li, F.-S. Yu, and C.-D. Lu, Analysis of two-body charmed B meson decays in factorization-assisted topological-amplitude approach, Phys. Rev. D **92**, 094016 (2015).

[77] S.-H. Zhou, Q.-A. Zhang, W.-R. Lyu, and C.-D. Lü, Analysis of charmless two-body B decays in factorization assisted topological amplitude approach, Eur. Phys. J. C **77**, 125 (2017).

[78] H.-Y. Jiang, F.-S. Yu, Q. Qin, H.-n. Li, and C.-D. Lü, D^0-$\bar{D}^0$ mixing parameter y in the factorization-assisted topological-amplitude approach, Chin. Phys. C **42**, 063101 (2018).

[79] D. Wang, F.-S. Yu, P.-F. Guo, and H.-Y. Jiang, $K_S^0 - K_L^0$ asymmetries in D-meson decays, Phys. Rev. D **95**, 073007 (2017).

[80] S.-H. Zhou and C.-D. Lü, Extraction of the CKM phase γ from the charmless two-body B meson decays, Chin. Phys. C **44**, 063101 (2020).

[81] S.-H. Zhou, R.-H. Li, Z.-Y. Wei, and C.-D. Lu, Analysis of three-body charmed B-meson decays under the factorization-assisted topological-amplitude approach, Phys. Rev. D **104**, 116012 (2021).

[82] S.-H. Zhou, X.-X. Hai, R.-H. Li, and C.-D. Lu, Analysis of three-body charmless B-meson decays under the factorization-assisted topological-amplitude approach, Phys. Rev. D **107**, 116023 (2023).

[83] S.-H. Zhou, R.-H. Li, and X.-Y. Lü, Analysis of three-body decays B → D(V →)PP under the factorization-assisted topological-amplitude approach, Phys. Rev. D **110**, 056001 (2024).

[84] S.-H. Zhou *et al.*, Updated analysis of $D \to PV$ under the factorization-assisted topological-amplitude approach (to be published).

[85] H.-Y. Cheng and C.-W. Chiang, Updated analysis of $D \to PP, VP$, and VV decays: Implications for $K_S^0 - K_L^0$ asymmetries and D^0-$\bar{D}^0$ mixing, Phys. Rev. D **109**, 073008 (2024).

[86] Y. Li, W.-F. Wang, A.-J. Ma, and Z.-J. Xiao, Quasi-two-body decays $B_{(s)} \to K^*(892)h \to K\pi h$ in perturbative QCD approach, Eur. Phys. J. C **79**, 37 (2019).

[87] A.-J. Ma, W.-F. Wang, Y. Li, and Z.-J. Xiao, Quasi-two-body decays $B \to DK^*(892) \to DK\pi$ in the perturbative QCD approach, Eur. Phys. J. C **79**, 539 (2019).

[88] Y.-Y. Fan and W.-F. Wang, Resonance contributions $\phi(1020, 1680) \to K\bar{K}$ for the three-body decays $B \to K\bar{K}h$, Eur. Phys. J. C **80**, 815 (2020).

[89] A.-J. Ma and W.-F. Wang, Contributions of the kaon pair from $\rho(770)$ for the three-body decays $B \to DK\bar{K}$, Phys. Rev. D **103**, 016002 (2021).

[90] W.-F. Wang, Contributions for the kaon pair from $\rho(770)$, $\omega(782)$ and their excited states in the $B \to K\bar{K}h$ decays, Phys. Rev. D **103**, 056021 (2021).

[91] W.-F. Wang, L.-F. Yang, A.-J. Ma, and A. Ramos, Low-mass enhancement of kaon pairs in $B^+ \to \bar{D}^{(*)0} K^+ \bar{K}^0$ and $B^0 \to D^{(*)-} K^+ \bar{K}^0$ decays, Phys. Rev. D **109**, 116009 (2024).

[92] J. M. Blatt and V. F. Weisskopf, *Theoretical Nuclear Physics* (Springer, New York, 1952).

[93] R. Aaij *et al.* (LHCb Collaboration), Dalitz plot analysis of $B_s^0 \to \bar{D}^0 K^- \pi^+$ decays, Phys. Rev. D **90**, 072003 (2014).

[94] R. Aaij *et al.* (LHCb Collaboration), Amplitude analysis of $B^- \to D^+ \pi^- \pi^-$ decays, Phys. Rev. D **94**, 072001 (2016).

[95] R. Aaij *et al.* (LHCb Collaboration), Amplitude analysis of the $B^+ \to \pi^+ \pi^+ \pi^-$ decay, Phys. Rev. D **101**, 012006 (2020).

[96] S. Navas *et al.* (Particle Data Group), Review of particle physics, Phys. Rev. D **110**, 030001 (2024).

[97] H.-Y. Cheng and C.-K. Chua, Branching fractions and direct CP violation in charmless three-body decays of B mesons, Phys. Rev. D **88**, 114014 (2013).

[98] C. Bruch, A. Khodjamirian, and J. H. Kuhn, Modeling the pion and kaon form factors in the timelike region, Eur. Phys. J. C **39**, 41 (2005).

[99] D. Besson *et al.* (CLEO Collaboration), Improved measurements of D meson semileptonic decays to pi and K mesons, Phys. Rev. D **80**, 032005 (2009).

[100] L. Widhalm *et al.* (Belle Collaboration), Measurement of $D^0 \to \pi l \nu (K l \nu)$ form factors and absolute branching fractions, Phys. Rev. Lett. **97**, 061804 (2006).

[101] M. Ablikim *et al.* (BESIII Collaboration), First measurement of the form factors in $D_s^+ \to K^0 e^+ \nu_e$ and $D_s^+ \to K^{*0} e^+ \nu_e$ decays, Phys. Rev. Lett. **122**, 061801 (2019).

[102] M. Ablikim *et al.* (BESIII Collaboration), Improved measurement of the semileptonic decay $D_s^+ \to K^0 e^+ \nu_e$, Phys. Rev. D **110**, 052012 (2024).

[103] C. Bernard *et al.*, Visualization of semileptonic form factors from lattice QCD, Phys. Rev. D **80**, 034026 (2009).

[104] D.-S. Du, J.-W. Li, and M.-Z. Yang, Form-factors and semileptonic decay of $D_s^+ \to \phi \bar{l} \nu$ from QCD sum rule, Eur. Phys. J. C **37**, 173 (2004).

[105] H.-J. Tian, Y.-L. Yang, D.-D. Hu, H.-B. Fu, T. Zhong, and X.-G. Wu, Searching for $|V_{cd}|$ through the exclusive decay $D_s^+ \to K^0 e^+ \nu_e$ within QCD sum rules, Phys. Lett. B **857**, 138975 (2024).

[106] D. Melikhov and B. Stech, Weak form-factors for heavy meson decays: An update, Phys. Rev. D **62**, 014006 (2000).

[107] C.-H. Chen, Y.-L. Shen, and W. Wang, $|V_{ub}|$ and $B \to \eta^{(\prime)}$ form factors in covariant light front approach, Phys. Lett. B **686**, 118 (2010).

[108] R. C. Verma, Decay constants and form factors of s-wave and p-wave mesons in the covariant light-front quark model, J. Phys. G **39**, 025005 (2012).

[109] W. Wang and Y.-L. Shen, $D_s \to K, K^*, \phi$ form factors in the covariant light-front approach and exclusive D_s decays, Phys. Rev. D **78**, 054002 (2008).

[110] D.-D. Hu, X.-G. Wu, L. Zeng, H.-B. Fu, and T. Zhong, Improved light-cone harmonic oscillator model for the ϕ-meson longitudinal leading-twist light-cone distribution

amplitude and its effects to $D_s^+ \to \phi \ell^+ \nu \ell$, Phys. Rev. D **110**, 056017 (2024).

[111] S. Fajfer and J. F. Kamenik, Charm meson resonances and $D \to V$ semileptonic form-factors, Phys. Rev. D **72**, 034029 (2005).

[112] S. Momeni and M. Saghebfar, Semileptonic D meson decays to the vector, axial vector and scalar mesons in Hard-Wall AdS/QCD correspondence, Eur. Phys. J. C **82**, 473 (2022).

[113] H. A. Ahmed, Y. Chen, and M. Huang, D_s- mesons semileptonic form factors in four-flavor holographic QCD, Phys. Rev. D **109**, 026008 (2024).

[114] Y. Fu-Sheng, X.-X. Wang, and C.-D. Lu, Nonleptonic two body decays of charmed mesons, Phys. Rev. D **84**, 074019 (2011).

[115] B. Aubert *et al.* (*BABAR* Collaboration), Measurement of CP violation parameters with a Dalitz plot analysis of $B^\pm \to D_{\pi^+\pi^-\pi^0} K^\pm$, Phys. Rev. Lett. **99**, 251801 (2007).

[116] A. Kuzmin *et al.* (Belle Collaboration), Study of $\bar{B}^0 \to D^0 \pi^+ \pi^-$ decays, Phys. Rev. D **76**, 012006 (2007).

[117] R. Aaij *et al.* (LHCb Collaboration), Amplitude analysis of $B^- \to D^+ \pi^- \pi^-$ decays, Phys. Rev. D **94**, 072001 (2016).